Scanning Photocurrent Imaging and Electronic Band Studies in Silicon Nanowire Field Effect Transistors

Yeonghwan Ahn, James Dunning, and Jiwoong Park*
The Rowland Institute at Harvard, Cambridge, Massachusetts 02142
(Dated: February 25, 2005)

We report optical scanning measurements on photocurrent in individual Si nanowire field effect transistors (SiNW FETs). We observe increases in the conductance of more than two orders of magnitude and a large conductance polarization anisotropy of 0.8, making our SiNW FETs a polarization sensitive, high resolution light detector. In addition, scanning images of photocurrent at various biases reveal the local energy band profile especially near the electrode contacts. The magnitude and polarity of the photocurrent vary depending on gate bias, a behavior that can be explained using the band flattening and a Schottky barrier type change. This technique is a powerful tool for studying photo-sensitive nanoscale devices.

PACS numbers: 73.63.-b,72.40.+w,73.40.Cg

Semiconducting nanoscale structures, especially nanowires (NWs) [1] and carbon nanotubes (CNTs) [2, 3], offer exciting electronic and optical properties, and have been recently used as a core material in several optoelectronic components. In particular, photoconductance measurements have been performed on InP [4], ZnO [5], and GaN [6] NWs as well as on CNTs [7, 8], proving their potential applications for high resolution, polarization sensitive photodetectors. Optical studies on SiNWs however, have primarily focused on the confinement effects using photoluminescence measurements [9, 10].

In most previous studies, the characteristics of individual NW or CNT optoelectronic devices were measured with a wide-field illumination, which lacks the capability to locally probe and measure light-induced responses. It is widely known that devices fabricated using semiconducting NWs or CNTs form non-Ohmic contacts and therefore their contact properties play a crucial role in understanding the overall performance [11–14]. Therefore, the development of a local optical probe technique is highly desirable for investigating how contact properties and the overall electronic band profile affect the device characteristics. Recently, scanning photoelectric measurements were demonstrated using CNT devices [8], but the spatial profile of the electronic band in individual NWs has not been investigated in conjunction with their photoelectronic properties.

We report scanning measurements of photoconductance and photocurrents in Si nanowire FETs. We show that Si nanowires can be used as a polarization sensitive, high resolution photodetector in the visible range. We also show that the local optoelectronic characteristics provide the detailed spatial information on the energy band diagram in our SiNW FETs.

Fabrication of SiNW FETs begins with the synthesis of nanowires using the vapor-liquid-solid chemical vapor deposition technique [15]. Au clusters (∼20 nm) were used as a catalyst to grow SiNWs in a flow of SiH_4 and H_2. A small amount of B_2H_4 was sometimes mixed into the flow in order to grow p-doped NWs. Both intrinsic and p-type NWs were 20∼40 nm thick (measured by AFM) and had a single crystalline core (confirmed by TEM). SiNWs were then deposited on a Si wafer substrate with a 220 nm thick thermal oxide layer that serves as a gate oxide. The conducting substrate was used as a back gate. Both standard photo- and electron-beam lithography techniques were used to define electrical contacts. To improve the contact properties, we used a 50 nm thick Ni layer to contact SiNWs with a rapid thermal annealing process.

The combined optical scanning microscope and transport measurement is illustrated in FIG 1a. In this setup, a SiNW device can be illuminated by a scanning diffraction-limited laser spot (diameter ∼ 500 nm) with a wavelength of 532 nm while the device conductance is recorded in ambient conditions. The small spot size of the light enables us to record the photo-induced electronic signal that originates from different parts of SiNWs. We can also simultaneously measure the reflected light to determine the absolute position of the laser spot.

In FIG 1b-d, we first show the scanning photoconductance (PC) recorded for a short (∼0.8 μm) p-type SiNW device. With the light linearly polarized parallel to the axis of the NW, the device shows a large conductance change only when the light spot is located on the NW (main panel, FIG 1b). On the other hand, when the light is polarized perpendicular to the NW axis, a much smaller PC was observed (upper inset, FIG 1b). FIG 1c shows the PC (denoted by ΔG) as a function of the light intensity (at the maximum conductance change position). The PC increases linearly with the light intensity for more than two orders of magnitude with a sensitivity that is similar to that of InP NWs previously reported [4] and significantly larger than that of CNTs [7]. In FIG 1d, we show the polar plot of the PC versus the polarization of the incident light. This clearly shows that the

*Electronic address: park@rowland.harvard.edu

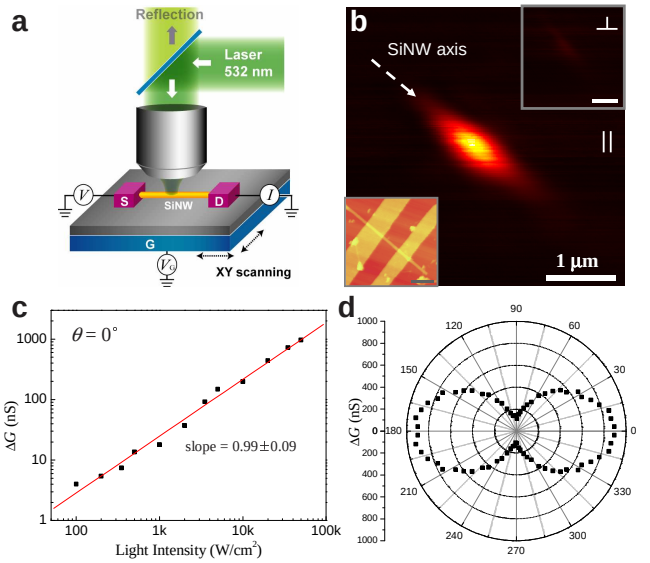

FIG. 1: (a) The scanning photocurrent measurement setup. (b) Scanning PC images measured at $V = 0.1$ V with the light polarization parallel (main panel) and perpendicular (upper inset) to the NW. The nanowire PC is represented by the color scale which increases from black (0 nS) through red to yellow (1000 nS). The lower inset shows a topographic AFM image of the device. (1 μm scale bars in the insets) (c) The light instensity and (d) polarization dependence of the SiNW PC with the laser spot at the maximum in the main panel of (b). In (d), zero corresponds to the parallel polarization. The PC was measured only between zero and 180 degrees and then copied to the other half.

NW conductance is the maximum (minimum) when the polarization of the incident light is parallel (perpendicular) to the axis of the NW. The PC anisotropy ratio, $\sigma = (\Delta G_{\parallel} - \Delta G_{\perp})/(\Delta G_{\parallel} + \Delta G_{\perp})$ of this device is 0.8.

These observations show that SiNW devices are excellent polarization sensitive light detectors with a submicron spatial resolution. The observed PC anisotropy is most likely due to the anisotropy in the light absorption, which is caused by a large dielectric contrast between SiNW ($\varepsilon = 11.8$) and its surroundings ($\varepsilon \sim 1$). This has been previously cited as the principal mechanism for the photoluminescence and photoconductance polarization anisotropy observed from InP and Si nanowires with a wide-field illumination [4, 10].

However, a more intriguing photoelectric behavior was observed when we measured longer SiNWs whose length is much larger than the size of the laser spot. In FIG 2a, we overlay two images measured simultaneously. The first image, represented by a gray scale, shows the confocal image of the reflected light measured with the same 532 nm laser. Large gold electrodes are visible in the light gray areas on either side of the SiNW (indicated using a white dotted line based on the AFM topographic image). The second image, represented by a color scale, shows electric current as a function of the laser spot position when $V = 0$. Here, red (blue) indicates a positive

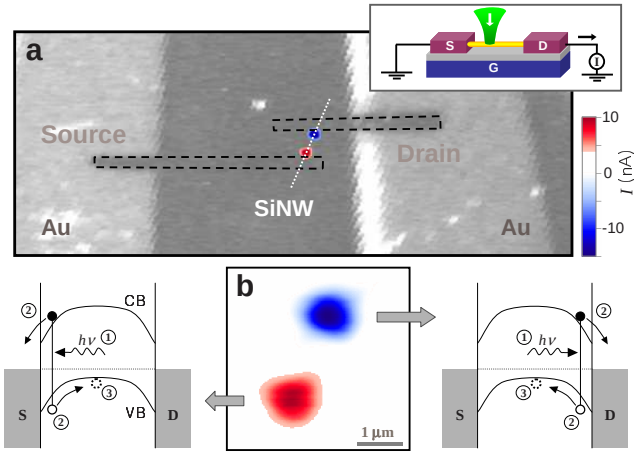

FIG. 2: (a) A scanning photocurrent image (color scale) overlaid over a confocal reflection image (gray scale) simultaneously taken at $V = V_G = 0$ with the light intensity of 100 kW/cm^2. The image size is 20 by 50 μm. In the reflection image, Ni electrodes are highlighted by dashed lines. (b) An enlarged photocurrent image from (a) with energy band diagrams describing the mechanism of the SPC generation.

(negative) current. A localized positive current spot near the source electrode as well as a negative current spot near the drain electrode is clearly visible in FIG 2a.

These light-induced current "pockets" near the contacts were observed at zero bias from all SiNW devices (more than ten devices) measured to date with magnitude ranging from 10 to 50 nA for a light intensity of $\sim$ 100 kW/cm^2 at $V_G = 0$ V. More interestingly, it always shows positive (negative) current with the laser spot close to the source (drain) electrode. The magnitude of the current spot is linearly proportional to the light intensity and shows similar light polarization dependence as in FIG 1d, another behavior that strongly suggests this localized photocurrent originates from the wire itself.

This striking zero-bias photocurrent behavior can be explained from a simple process shown in FIG 2b. If a SiNW is illuminated near the source electrode (left diagram), electron-hole pairs will be locally created (1). Then they will be accelerated in opposite directions, i.e. electrons to the source electrode, holes to the middle of the wire driven by the electric field near the electrode contact (2). We draw the electronic bands to be lower near the contacts to match the observed photocurrent polarity (see below). The electrons injected into the source electrode will contribute to net positive (zero) current when holes are annihilated by electrons originating from the drain (source) contact (3). As a result, net positive current will flow. The same process will produce a negative current with the light near the drain electrode (right diagram), and its polarity will not change as long as the electronic energy is lower near the contacts than in the middle of the nanowire. To our knowledge, this Schottky photocurrent (SPC) behavior, whose current generating mechanism is similar to that of the Schottky photodiode

[16], has not been studied previously in nanowire devices.

Because the SPC and the electronic band profile are closely related, we can easily deduce properties of SiNW electronic band using the behavior of the NW SPC. First, it is clear from the universal presence of the SPC, that the electronic band in all our NW devices is bent near metal contacts. Second, the direction of the bending near contacts is in the same direction for intrinsic and p-doped NWs since the polarity of the SPC is device independent. In particular, all SiNWs in our devices form an accumulation layer at the Ni contacts near zero gate voltage. The magnitude and the polarity of the SPC can be more quantitatively expressed by a simple equation [16],

$$i_{\mathrm{SPC}} = |e|N(P_{\mathrm{S}}^{e} - P_{\mathrm{S}}^{h}) = -|e|N(P_{\mathrm{D}}^{e} - P_{\mathrm{D}}^{h}) \qquad (1)$$

where N is the number rate of the electron-hole pairs generated by the light and $P_{\mathrm{S(D)}}^{e(h)}$ is the probability that a photo-excited electron (hole) is transported to the source (drain) electrode. In our experiment, N will vary depending on the light intensity, light polarization, and the volume of the nanowire under illumination. Also important is the skin depth of Si, which is ~ 1 μm, at the wavelength of the laser. Based on our experimental conditions, we estimate the typical value for $|e|N$ to be around 500 nA, which indicates that the SPC detection efficiency is as large as 10 %. This is a large value considering that we have not performed any surface treatment for the NW to optimize the efficiency.

In FIG 3, we study the gate dependence of the SPC. First, scanning SPC images taken at different gate voltages show a clear polarity switching behavior (see FIG 3a). The white spot (positive SPC) located near the source at negative gate voltage vanishes in the middle image and then reappears at large positive gate voltages as a black spot (negative SPC). The same behavior is also clearly seen in FIG 3b. The polarity switching of the SPC strongly indicates that the bending direction of the electronic band switches at large gate voltages as illustrated in the band diagrams in the insets. In FIG 3b, we also note that polarity switching of both SPC spots occur at approximately the same gate bias (marked by an arrow) and that the magnitude of the SPC changes almost linearly for a wide gate voltage range (for example, from -10 to 10 V). The latter behavior suggests that the magnitude of the SPC can be used as a local probe for the bending steepness of the electronic band.

From the gate dependence of the SPC together with the DC conductance measurement, we can determine a SiNW electronic band parameter as described below. First, we determine the efficiency of the gate potential $\alpha = |\Delta E/e\Delta V_{\mathrm{G}}|$ (ΔE, the electron band energy change) from the slope of the exponential DC conductance falloff in the subthreshold gate region (inset, FIG 3c) [17]. The DC conductance of the NW is measured in the absence of light. Using the measured gate voltages for the p-type conductance shut-off (~ 0 V, arrow in FIG 3c) and the electronic band flattening (~ 15 V, arrow in FIG 3b) together with $\alpha = 0.037$ and the Si bandgap Eg = 1.12 eV,

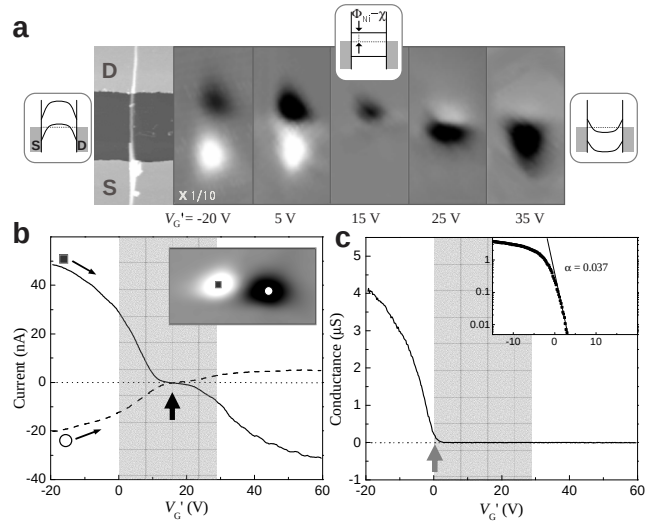

FIG. 3: (a) A series of grayscale (white corresponding to the positive current) scanning SPC images (4×2 μm) taken at different gate voltages. An AFM image of the device is shown on the left. (b) The SPC vs gate voltage. The inset (taken at the zero gate bias) shows the location of the laser spot for each line plots. (c) The DC conductance at $V = 10$ mV in the absence of light. The inset shows a semi-logarithmic plot of the main panel. This is used to determine the band-gap region which is represented by the shaded area in (b) and (c). In (a) through (c), the gate axis is corrected for the systematic gate shift caused by the previous gate scans.

we determine the electron barrier height $\Phi_{\mathrm{Ni}} - \chi$ (see the middle band diagram in FIG 3a) at the Ni/SiNW contact to be 0.57 eV. This is in good agreement with a tabulated value 0.61 eV for the Ni/Si contact in bulk samples [16].

Another intriguing observation in FIG 3a is the shrinking distance between the two SPC spots with increasing gate bias. For example, the center-to-center distance is measured at <0.5 μm from the fourth image, which is significantly shorter than that of the first image (~ 1.5 μm). This behavior contradicts the electrostatic potential calculations which predict that the band bending, if any, should be strongly confined near the contacts independent of the gate voltage [11]. This unusual behavior is likely caused by the field screening due to various surface and impurity charges near the contacts. This effect has been frequently cited as a cause for several non-ideal device characteristics, especially if the devices are not suitably passivated [18–20]. In addition, the n-type DC conductance is completely missing in the device shown here, which is consistent with the behavior explained above.

Finally, we study the bias dependence of the SPC. Surprisingly, we find that the SPC dominates the photoelectric signal for many SiNW devices even when a large bias was applied. FIG 4 shows the scanning photocurrent images (middle column) measured at different bias voltages (from 0.2 V to -0.2 V, top to bottom) for the same device as in FIG 2. The SPC spots are clearly visible with their circular shape and the center position roughly the

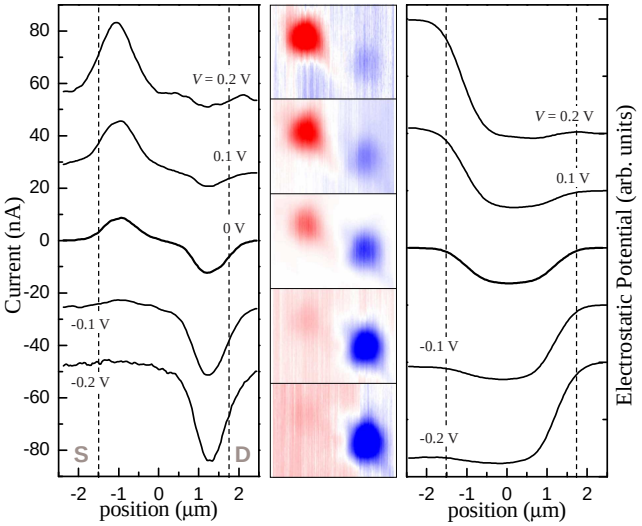

FIG. 4: Bias dependence of the SPC. (Middle column) Color scale scanning photocurrent images (3×4 μm) for different bias voltages. Red (blue) corresponds to the maximum (minimum) current. (Left column) Cross-sectional photocurrent line plots along the NW axis, each offset by 10 nA. (Right column) Electrostatic potential calculated from the left column (offset for clarity).

same at all biases. However, the intensity of the positive (negative) SPC spot becomes weaker at negative (positive) biases, finally vanishing near -0.2 V (0.2 V). Also notable is the fact that no significant photo-induced current is observed when the light is focused on the middle of the NW. These behaviors are most likely due to a large potential drop near the contacts as well as a relatively flat band in the middle of the SiNW as supported by the electrostatic potential profile calculated using FEMLAB.

In fact, our scanning SPC measurement, especially its polarity, can be used to probe the behavior of the local electrostatic potential, especially its ups and downs. It is also likely that the intensity of the SPC will be roughly proportional to the local electric field (equivalently the steepness of the potential) as discussed earlier. Therefore, the spatial map of the electrostatic potential profile can be qualitatively captured by integrating the SPC line scans shown on the left side. The electrostatic potential profile calculated this way is shown along the NW axis in the right column. We can clearly see in which direction the potential is bent and also where it becomes level.

In conclusion, we have measured the photoconductance and photocurrent in individual SiNW FETs using the combined optical scanning microscope and transport measurement setup. We observe a surprisingly strong photocurrent near the contacts, which originates from the electronic band bending. The behavior of this photocurrent was investigated at different gate and source-drain biases, revealing its potential application as a scanning probe for the electronic band structure within the nanowire. This unique photoelectric phenomenon could also be used to fabricate a highly sensitive point photodetector, which could find applications for high resolution position sensors, local biosensor for optically active species, and advanced photosensitive scanning probe tips.

We thank C. M. Lieber, B. Timko, W. Hill, and C. Stokes for their help in setting up the nanowire growth setup. We also thank M. Burns for his help on the electrostatic potential calculations and helpful discussions. This work was fully supported by the Rowland Junior Fellowship program.

[1] C. M. Lieber, MRS Bulletin **28**, 486 (2003).
[2] P. L. McEuen and J. Y. Park, MRS Bulletin **29**, 272 (2004).
[3] P. Avouris, MRS Bulletin **29**, 403 (2004).
[4] J. F. Wang et al., Science **293**, 1455 (2001).
[5] H. Kind *et al.*, Adv. Mater. **14**, 158 (2002).
[6] S. Han *et al.*, Chem. Phys. Lett. **389**, 176 (2004).
[7] M. Freitag *et al.*, Nano Lett. **3**, 1067 (2003).
[8] K. Balasubramanian *et al.*, Appl. Phys. Lett. **84**, 2400 (2004).
[9] Z. G. Bai *et al.*, Mater. Sci. Eng. B **72**, 117 (2000).
[10] J. Qi *et al.*, Appl. Phys. Lett. **82**, 2616 (2003).
[11] S. Heinze *et al.*, Phys. Rev. Lett. **89**, 106801 (2002).
[12] J. Appenzeller *et al.*, Phys. Rev. Lett. **89**, 126801 (2002).
[13] A. Javey *et al.*, Phys. Rev. Lett. **92** 106804 (2004).
[14] Y. Yaish *et al.*, Phys. Rev. Lett. **92** 046401 (2004).
[15] Y. Cui *et al.*, Appl. Phys. Lett. **78**, 2214 (2001).
[16] S. M. Sze, *Physics of Semiconductor Devices* (John Wiley & Sons, 1981).
[17] S. Rosenblatt *et al.*, Nano Lett. **2**, 869 (2002).
[18] Y. Cui *et al.*, Nano Lett. **3**, 149 (2003).
[19] W. Kim *et al.*, Nano Lett. **3**, 193 (2003).
[20] G. W. Neudeck and R. F. Pierret, *Field Effect Devices* (Addison-Wesley Publishing Company, 1990).